Mechatronics 113 (2026) 103422

Contents lists available at ScienceDirect

Mechatronics

journal homepage: www.elsevier.com/locate/mechatronics

Learning feedforward with unmeasured performance variables: With application to a wirebonder☆,☆☆

Maurice Poot [a], Jorrit Sprik [a], Matthijs Teurlings [a], Wout Laarakkers [b], Dragan Kostić [b], Jim Portegies [c], Tom Oomen [a,d,*]

[a] Department of Mechanical Engineering, Eindhoven University of Technology, PO Box 513, Eindhoven, 5600MB, The Netherlands
[b] Centre of Competency, ASMPT, Platinawerf 20, Beuningen, 6641TL, The Netherlands
[c] Department of Mathematics and Computer Science, Eindhoven University of Technology, PO Box 513, Eindhoven, 5600MB, The Netherlands
[d] Delft Center for Systems and Control, Delft University of Technology, Mekelweg 2, Delft, 2628CD, The Netherlands

ARTICLE INFO

Keywords:
Unmeasured performance variable
Wirebonder
Motion control
Iterative learning control
Sensor fusion

ABSTRACT

Feedforward motion control for unmeasured performance variables at the point of interest is crucial for attaining high throughput and accuracy in motion systems. The aim of this paper is to develop a data-driven approach for feedforward tuning that addresses the true performance at the point of interest. The presented approach is a novel methodology that employs rational feedforward structures for performing flexible tasks with high accuracy, in conjunction with an sensor fusion for addressing the point-of-interest. In particular, the tracking error of the unmeasured performance variable is accurately estimated by combining acceleration measurements and encoder measurements. Simulation results show that optimizing for the estimated point-of-interest error achieves similar tracking performance as optimizing for the true point-of-interest error, indicating accurate sensor-fusion estimates for feedforward control. Experimental validation demonstrates that optimizing for the estimated point-of-interest error significantly reduces the estimated point-of-interest tracking error compared to minimizing the encoder error.

1. Introduction

Motion control for unmeasured performance variables, often referred to as point-of-interest or inferential control, is crucial for achieving high accuracy and throughput in advanced motion systems. General control applications with such unmeasured performance variables are widespread, including heat exchangers and industrial autoclave processes [1], robotics [2], and mechatronics [3]. Examples of mechatronic systems with unmeasured performance variables include wirebonding machines [4], which create interconnections between integrated circuits and the external world via a small bond head. Typical in these machines, sensors producing measured variables for feedback and feedforward control, such as optical encoders, cannot be directly positioned in the bond head, i.e., the point of interest [3]. This leads to a discrepancy between the *measured position* and the actual *point-of-interest position* where performance is desired [5]. These differences are often ignored or overlooked due to the challenges of obtaining accurate measurements or obtaining reliable models. As a result, current control methodologies tend to focus only on the measured performance in the encoder, resulting in a possible, yet often unrecognized, performance loss at the point of interest. To achieve high tracking performance at the point of interest, accurate estimation of the point of interest and accurate control methodologies, including feedback and feedforward control, of the point of interest are necessary [6,7].

In recent years, data-driven feedforward algorithms have been developed that employ measured data, typically at the measured variables [8]. For the restrictive case of trial-invariant references, data-driven learning of high-accuracy feedforward signals has been enabled through iterative learning control (ILC) [9]. In ILC, past trial data and an approximate model of the system are used to iteratively learn a feedforward signal. In norm-optimal ILC (NOILC) [10], a specific class of ILC, a convex optimization problem is solved in each iteration to minimize the next trial's error. Despite the high-tracking accuracy of ILC, widespread industrial adoption of ILC is hampered by the key assumption on trial-invariant motion tasks, as extrapolation to other tasks generally leads to significant performance deterioration [11].

☆ This work is supported by ASMPT.
☆☆ This paper was recommended for publication by Associate Editor Toru Namerikawa.
* Corresponding author.
E-mail address: t.a.e.oomen@tue.nl (T. Oomen).

https://doi.org/10.1016/j.mechatronics.2025.103422
Received 6 November 2024; Received in revised form 16 September 2025; Accepted 16 October 2025
Available online 28 October 2025

The industrial need for motion task flexibility has spurred the development of task-flexible ILC approaches. In [12], the motion task is divided into sub-tasks that are learned individually, but this restricts the motion task to a predefined library. Additionally, in [13], the feedforward signal is parameterized in terms of the motion task using polynomial basis functions, these basis functions can be interpreted as representing the inverse system using a finite impulse response (FIR) filter, see [11]. However, this polynomial feedforward parameterization tacitly assumes that the system has a unit numerator, which is not typical for physical systems with flexible dynamics, leading to under-modeling and poor tracking accuracy and extrapolation properties. To improve accuracy and extrapolation properties, ILC has been extended with rational basis functions [14], resulting in a non-convex optimization problem. Locally optimal solutions can be obtained by iteratively solving the non-convex optimization problem using a gradient-based weighting, solving a series of weighted least-squares problems [15], which connects to instrumental variable-based system identification, see [16]. These feedforward approaches achieve high-tracking accuracy and task flexibility, but are primarily focused on measured variables. This may adversely affects performance at the point of interest due to dynamic differences, leading to the inferential motion control problem.

Data-driven feedforward methodologies typically employ measured error signals, which are often not equal to the point-of-interest. This inferential control situation with unmeasured point-of-interest variables is far from trivial, since utmost care must be taken that the feedback controller that uses the measured variables does not interfere with the performance variables. Conceptually, the unmeasured point-of-interest variable can be estimated from the measured variables through the use of a model [7], but this often leads to inherent inaccuracies due to difficult-to-model dynamics. The model uncertainty has been accounted for in feedback control through robust inferential control approaches [3]. Feedforward control methods, including ILC, have also been applied in an inferential control context. In [17], a Kalman filter-based ILC approach is developed and in [2] an analysis of its convergence properties is given. However, this does not address the task-flexible requirement in typical motion applications. A more general framework based on 2D system theory that identifies the potential challenges with a combined ILC and feedback situation is developed in [5], but its actual design, in particular for task-flexible situations is not addressed. Finally, in [6], the feedback and feedforward are jointly optimized, but such approaches are not compatible with the different requirements on feedforward and feedback controllers, and do not directly extend to a task-flexible situation as well.

Although high tracking accuracy and task flexibility can be achieved with current ILC methodologies, these methods are not designed for inferential control of unmeasured point-of-interest variables. Furthermore, estimation of these unmeasured point-of-interest variables is non-trivial and challenging, especially with limited or no model knowledge. Also, the inferential control situation is not straightforward, since care has to be taken that the feedback and feedforward do not interfere with each other's objectives. The aim of this paper is to develop a data-driven rational feedforward tuning approach for unmeasured performance variables using sensor fusion. By estimating these variables through offline filtering in a batch-to-batch process, incorporating temporary acceleration measurements and measured signals, reliable estimates of the point-of-interest tracking error are generated. Subsequently, these estimates are optimized in a rational basis functions ILC framework to achieve high tracking accuracy and task flexibility.

The main contribution in this paper is a data-driven framework for rational feedforward tuning for unmeasured performance variables using ILC and sensor fusion. The sub-contributions are as follows.

I A general framework for data-driven rational feedforward tuning using ILC and offline sensor fusion to address point-of-interest performance.

II Sensor fusion framework for estimation of performance variable from acceleration measurements, including design and implementation aspects, which ensures that the feedback and feedforward controller do not interfere in the sense of [5].

III A simulation study that confirms the estimation performance of sensor fusion.

IV An experimental validation on a commercial wirebonder that confirms superior performance compared to the state of practice.

This framework facilitates rapid commissioning and industry adoption by enabling data-driven learning of high-performance feedforward controllers through user-friendly offline estimation.

This paper is structured as follows. The notation used in this paper is presented in the following section. In Section 2, the problem is formulated. The developed approach is presented in Section 3, where the entire section constitutes Contribution I, and Section 3.1 contains Contribution II. In Section 4, a simulation study is presented, which constitutes Contribution III. Then, in Section 5, the experimental implementation on the wirebonder is presented, constituting Contribution IV. Section 6 contains conclusions and future work.

Notation

All systems are assumed to be discrete-time (DT), linear, time-invariant (LTI), single-input, single-output (SISO) and are denoted by $\underline{H}(z)$ with complex indeterminate z. Signals are tacitly assumed to have length $N \in \mathbb{Z}^+$. The output $y(k)$ of the response of $\underline{H}(z)$ to input u is $y(k) = \sum_{l=-\infty}^{\infty} h(l)u(k-l)$, where $h(l)$ is the impulse response of the system $\underline{H}(z)$. When assuming $u(k) = 0$ for $k < 0$ and $k > N-1$, the response can be cast into a finite-time convolution as

$$\underbrace{\begin{bmatrix} y[0] \\ y[1] \\ \vdots \\ y[N-1] \end{bmatrix}}_{y} = \underbrace{\begin{bmatrix} h(0) & h(-1) & \cdots & h(1-N) \\ h(1) & h(0) & \cdots & h(2-N) \\ \vdots & \vdots & \ddots & \vdots \\ h(N-1) & h(N-2) & \cdots & h(0) \end{bmatrix}}_{H} \underbrace{\begin{bmatrix} u[0] \\ u[1] \\ \vdots \\ u[N-1] \end{bmatrix}}_{u}, \tag{1}$$

with $u, y \in \mathbb{R}^N$ the input and output, respectively, and $H \in \mathbb{R}^{N \times N}$ the convolution matrix corresponding to $\underline{H}(z)$. Moreover, ith element of a vector x is denoted by $x[i]$, the shift operator q is defined as $q^{-1}y(t) := y(t-1)$, and the weighted 2-norm of a vector $x \in \mathbb{R}^n$ with positive semi-definite weighting matrix $W \in \mathbb{R}^{n \times n}$ is denoted by $\|x\|_W = \sqrt{x^\top W x}$.

2. Problem formulation

In this section, the problem is formulated. First, the control setting is described. Second, the challenges of estimating the point of interest are presented. Finally, the problem considered in this paper is formally stated.

2.1. Inferential control setting

Typical sensors of motion systems cannot be placed directly at the point of interest. For example, in a wirebonder, which creates interconnections on integrated circuits via a bond head, see Fig. 1, the point of interest where performance is desired is the bond head where bonding takes place. However, the measured variable that is used for control is typically a position reading from an optical encoder at a different location, see Fig. 3. This results in different dynamics between the measured variable and the performance variable. The desire to improve the tracking accuracy of the performance variable in the point of interest leads to an inferential motion control setting that requires accurate estimation and control of the performance variable instead of the measured variable that is used for feedback control.

The closed-loop control structure corresponding to the inferential motion control setting is depicted in Fig. 2, where the index j denotes

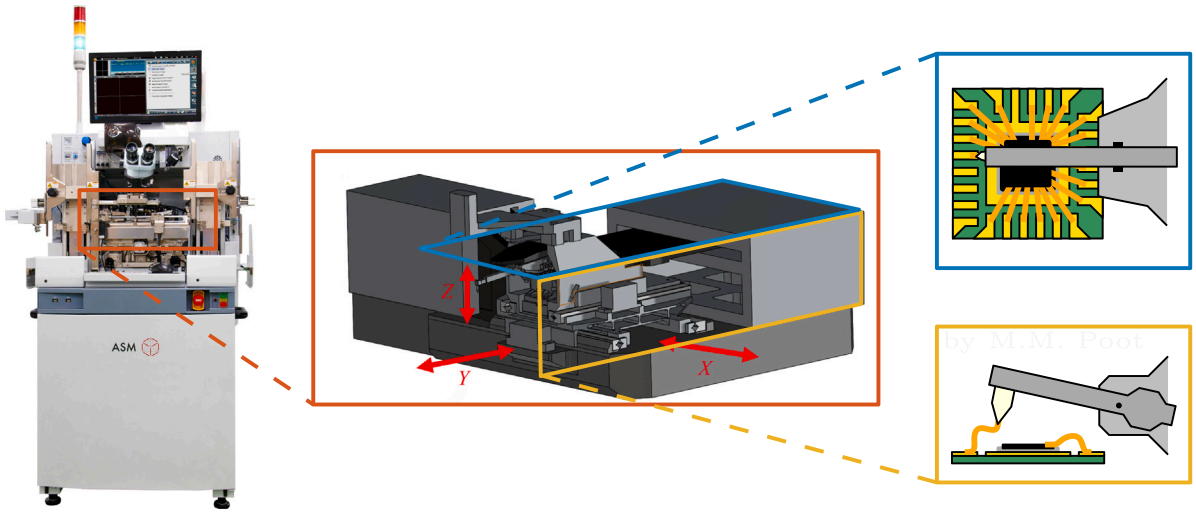

Fig. 1. Left: a commercial wirebonder machine by ASMPT. Center: 3D-model of the motion stage with three motion axes. Right: top and bottom schematic of a bond head above a chip.

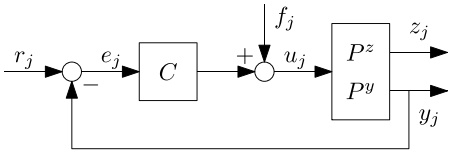

Fig. 2. Closed-loop control structure with feedforward f_j and measured output y_j used for feedback and unmeasured output of the point of interest z_j.

an experiment of length $N \in \mathbb{N}$. For a given reference $r_j \in \mathbb{R}^N$ and feedforward $f_j \in \mathbb{R}^N$, the measured output variable of the system is $y_j \in \mathbb{R}^N$ and the corresponding error signal of the measured variable used for feedback control is $e_j^y := r_j - y_j$. Now, the unmeasured performance variable, generally called the point of interest, is denoted by $z_j \in \mathbb{R}^N$, hence the system has one input $u_j \in \mathbb{R}^N$ and two outputs, y_j, z_j, of which the dynamics are described by P^y, P^z, respectively. Note that representations using a cascaded form, i.e., $u \to P^y \to \frac{P^z}{P^y}$ are also possible. The system P^y is controlled by a discrete-time and linear time-invariant feedback controller C and the closed-loop system is assumed to be stable.

The goal in inferential motion control is to design a feedforward signal f_j such that the point of interest z_j accurately tracks the reference r_j. This point of interest tracking error can be derived from Fig. 2 as

$$e_j^z := r_j - z_j = (1 - SP^zC)r_j - SP^zf_j, \tag{2}$$

where $S := (1 + P^yC)^{-1} : r \to e^y$ is the sensitivity of the closed-loop system.

Accurate tracking of r_j for the performance variable z_j is not evident, since, in contrast to current methods, a feedforward input should be optimized to achieve $e_j^z = 0$ instead of $e_j^y = 0$. The sensor of the measured variable y_j is often not located at the point of interest z_j, therefore, the dynamics for both outputs is different, i.e., $P^y \neq P^z$. Since $P^y \neq P^z$, achieving $e_j^y = 0$ generally results in $e_j^z \neq 0$, see [18], which means that optimizing for e_j^y may yield poor performance in z_j, and vice versa. This is illustrated in the tracking error in Fig. 10 of the results presented in Section 5. Furthermore, feedback controllers are generally tuned to optimize robustness and performance for e_j^y, hereby possibly amplifying flexible dynamics of P^z that results in poor tracking performance of the point of interest. This motivates the need to directly compensate for the error in e_j^z, instead of e_j^y, but gives rise to the need to estimate the unmeasured point of interest z_j, as described next.

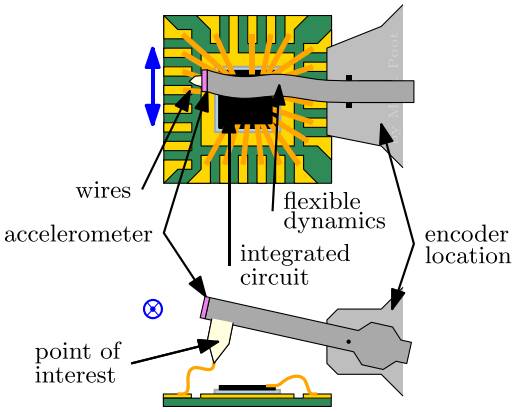

Fig. 3. Schematic of a wirebonder during operation, where the encoder location is a substantial distance from the unmeasured point-of-interest. An accelerometer is added to estimate the point of interest position for feedforward control. The motion direction of interest in the simulation study and experimental validation is highlighted by the blue arrow, and the top schematic exaggerates the flexible dynamics that are present in this motion direction.

2.2. Estimating the performance variable

To accurately control the performance variable, an accurate estimate of z is required, which is often difficult, troublesome, or expensive to obtain. As an example, an accelerometer is assumed to be attached to the point of interest, providing a cost-effective and decently reliable measurement of the point-of-interest acceleration. Accelerometers are widely used in control applications, see, e.g., [17,19]. Indeed, other options are available, e.g. laser interferometry, which is reliable and unintrusive but more expensive. The following assumption is made in case the accelerometer is temporary.

Assumption 1. The attached accelerometer does not significantly alter the dynamics of the point of interest, i.e., P^z remains approximately unchanged. □

Of course, if the sensor is not temporary, the unaltered dynamics become part of P^z and the approach remains valid.

Estimation of the point of interest position from the acceleration measurement is non-trivial. First, measurement noise influences the acceleration measurement, causing signal drift in the position estimation

when double integration of the acceleration data is performed. Second, an accurate model of the point-of-interest dynamics is often difficult or troublesome to obtain or inaccurate, making Kalman-filter-based techniques [20] undesirable. This leads to the problem considered in this paper.

2.3. Problem formulation

The problem defined in this paper is to achieve high tracking accuracy and task-flexibility at the point of interest. More specifically, the following two sub-problems are formulated.

- Estimate z_j from noisy acceleration data $\ddot{z}$ and encoder measurement y.
- Minimize e_j^z by designing f_j in a way that is task flexible.

Next, a solution for estimating the point-of-interest position and minimizing the tracking error are presented.

3. Approach

The main goal of this paper is to achieve high tracking accuracy and task flexibility at the point of interest, the developed approach employs offline sensor fusion of the measured variable y_j with the double integrated acceleration measurement to accurately estimate the position of the point of interest. This estimation is then utilized to minimize the tracking error at the point of interest through learning of a task-flexible feedforward signal using iterative learning control (ILC) with rational basis functions.

The outline of this section is as follows. The developed framework presented in this section constitutes the main methodological contributions of this paper, i.e., Contribution I and II. This section is structured as follows. In Section 3.1 the sensor fusion approach to estimate the point-of-interest error is presented, which constitutes Contribution II. Thereafter, in Section 3.2, the concept of ILC for the point of interest is first explained. Subsequently, the rational basis functions for task-flexible feedforward are introduced. At last, the solution for rational basis functions in ILC using sensor fusion is detailed, which constitutes Contribution I.

3.1. Estimation of the point of interest

To obtain a reliable estimate of the point-of-interest position z_j, sensor fusion is employed to combine two variables of the same physical quantity [21,22]. Here, this involves combining the double integrated acceleration measurement $\tilde{z}_j$ and the encoder measurement y_j. The former is expressed as

$$\tilde{z}_j = G_{\text{int}}^2 \left(\ddot{z}_j + v_j \right), \tag{3}$$

where G_{int} is the convolution matrix of an integrator and v_j is the measurement noise that causes drift in $\tilde{z}_j$ due to the integration. The double integration amplifies low-frequency noise, rendering acceleration measurements alone unreliable for estimating the point of interest. To enhance the accuracy of this estimation, sensor fusion is employed, combining $\tilde{z}_j$ with the encoder measurement y_j through a complementary filter [22], expressed as

$$\hat{z}_j = G_{\text{HP}} \tilde{z}_j + G_{\text{LP}} y_j. \tag{4}$$

Here, G_{HP} is the convolution of $G(q) \in \mathbb{R}[q]$ that represents a high-pass filter with shift operator q and a cut-off frequency ω_{co}. It ensures that the reliable high-frequency data of $\tilde{z}_j$ contributes to the estimate. Furthermore, G_{LP} is the convolution matrix of $1 - G(q)$, which is the complement of the high-pass filter such that only the low-frequency content of y_j is used for the estimation. In other words, the unreliable low-frequency content from the double integrated acceleration signal is substituted with the encoder measurement, effectively eliminating drift. This process operates under the following assumption.

Assumption 2. $P^z(z) \approx P^y(z) \forall \omega \ll 1$, i.e, the system P^z behaves similarly to P^y in the low-frequency range. □

This assumption holds true in many typical motion systems with point-of-interest dynamics due to the lightweight physical connection from the encoder to the point of interest, resulting in distinct dynamics primarily in the high-frequency range and dominant rigid-body mode in the low-frequency range.

The following statements can be made regarding the implementation and design aspects of the complementary filter. First, the frequency of the low- and high-pass filter, or the so-called cross-over frequency ω_{co}, should be selected sufficiently high to remove drift from the double integrated acceleration measurement, but should be below the frequency where P^y and P^z start to deviate. Second, to ensure that the magnitude of the signal remains the same when combining these separate measurements via (4), both filters should sum to one. Third, to avoid the introduction of phase delays through filtering, zero-phase filtering can be exploited [23], since the measurements are available offline. Fourth, to ensure that high frequency noise of the acceleration data does not affect the measurement, an additional, possibly zero-phase, low-pass filter can be used. Such zero-phase filtering [23] using any pair of high-pass and low-pass Butterworth filters will have zero-degree phase and a summed magnitude of one at any frequency, see Appendix B for details. At last, note that rotation calibration and gravity compensation of the accelerometer measurements might be necessary for accurate estimation results.

Remark 1. Sensor fusion via a complementary filter is a linear operation, hence connections to a Kalman filter [20,21] can be made, where the Kalman filter prediction model is a mass model, see [22]. Of course, Kalman filters, or more generally multiple sensors can be used through any filter or observer for broader applications, as long as these lead to an accurate estimate of the point of interest, in which case the learning approach of the forthcoming sections can be directly applied.

To conclude, accurate estimation of the point of interest is enabled by easy-to-tune sensor fusion of the double-integrated acceleration measurement and the measured variable. The estimate can be used to determine the point-of-interest tracking error, as defined as

$$e_j^{\hat{z}} := r_j - \hat{z}_j. \tag{5}$$

Finally, an estimate of the tracking error in the point of interest is available which can now be minimized through designing a task-flexible feedforward using ILC, as presented in the remainder of this section.

3.2. Minimizing the point-of-interest tracking error

To minimize the estimate of the point-of-interest tracking error of (5), a feedforward signal f_j needs to be designed. Here, ILC for point-of-interest control is derived that uses the sensor-fusion estimate of the point-of-interest tracking error to minimize the tracing error. Then, a feedforward parameterization is introduced that enables flexibility in the motion task. After that, the ILC optimization framework is presented that enables learning of the feedforward parameters to minimize the estimated point-of-interest tracking error.

3.2.1. ILC for point-of-interest control

In this section, ILC for point-of-interest measurements is developed, which is an essential step towards the flexible ILC approach in Section 3.2.2. The goal in standard ILC is to minimize the tracking error of the next trial at the point of interest, e_{j+1}^z, by learning f_{j+1}, in an iterative manner [9]. A key assumption in standard ILC is that the reference r is task-invariant, which will be relaxed in the next section to achieve task flexibility. The tracking error of the next trial is derived from (2), and is given by

$$e_{j+1}^z = (1 - SP^zC) r_{j+1} - SP^z f_{j+1}. \tag{6}$$

hence, the goal of ILC is to find f_{j+1} that minimizes this error. It is impossible to minimize e^z_{j+1} directly, since the system is unknown and only approximate models $\hat{S} = (I + \hat{P}^y C)^{-1}$ and $\hat{P}^z$ are known, where $\hat{P}^y$ is an approximate model of P^y. To fix this problem, the error is predicted using these approximate models. Given a trial index k and the models $\hat{S}$ and $\hat{P}^z$, the model-predicted error is defined as

$$\bar{e}^z_k := \left(1 - \hat{S}\hat{P}^z C\right) r_k - \hat{S}\hat{P}^z f_k. \tag{7}$$

Although it is possible to minimize this model-predicted error, results can be improved by compensating for inherent model mismatch by using the difference between the model-predicted error and the actual error from the previous iteration.

The key difference compared to traditional ILC, the actual error is unknown in ILC for point-of-interest control, and therefore the sensor fusion estimate of the point-of-interest error $e^{\hat{z}}_j$ of (5) is used instead. Thus, ILC for point-of-interest control minimizes $\tilde{e}^{\hat{z}}_{j+1} := \bar{e}^z_{j+1} - \left(\bar{e}^z_j - e^{\hat{z}}_j\right)$, which after substitution of (7) for both j and $j+1$ yields after rearranging

$$\begin{aligned}\tilde{e}^{\hat{z}}_{j+1} &:= e^{\hat{z}}_j - \left(1 - \hat{S}\hat{P}^z C\right) r_j + \hat{S}\hat{P}^z f_j \\ &\quad + \left(1 - \hat{S}\hat{P}^z C\right) r_{j+1} - \hat{S}\hat{P}^z f_{j+1}.\end{aligned} \tag{8}$$

The main point of (8) is that the error $e^{\hat{z}}_j$ follows directly from a measurement that employs sensor fusion, see (5), while the other terms are the past input signal f_j, known trajectories r_j and r_{j+1}, and the decision variable to be optimized f_{j+1}. By consecutively minimizing this error, an iterative scheme is obtained based on data from past trials that compensates for model mismatch, up to the prediction error of sensor fusion. Indeed, this is ILC, but using an estimate of the error. Similar to the standard ILC case, the terms with $\left(1 - \hat{S}\hat{P}^z C\right)$ cancel in case $r_{j+1} = r_j = r$, i.e., an iteration-invariant motion task. In that case, the predicted error propagation reduces to

$$\tilde{e}^{\hat{z}}_{j+1} := e^{\hat{z}}_j + \hat{S}\hat{P}^z f_j - \hat{S}\hat{P}^z f_{j+1}, \tag{9}$$

and can be iteratively minimized to learn f_{j+1}.

In traditional ILC, it is assumed that the reference is iteration invariant. This is not the case for the task-flexible case that is considered in the current paper, where f_j will be parameterized in the next section as a function of r_j due to the requirement on task flexibility.

Remark 2. It is important to realize that the entire data-driven optimization algorithm (8) uses the estimated point of interest $\hat{z}$, essentially through (5). Clearly, this requires an accurate observer. In particular, let the estimation error $\epsilon = \hat{z}_j - z_j$, where z_j is the true point-of-interest variable and $\hat{z}_j$ is the estimated point-of-interest variable that is used in the optimization. Then, if the estimated tracking error $e^{\hat{z}}_j$ in (5) is minimized, i.e., $e^{\hat{z}}_j = 0$, it immediately implies that the true error $r_j - z_j = \epsilon$, hence the estimation error directly remains, as intuitively could be expected. Clearly, this implies that the sensor fusion approach should only be used if the estimated point of interest $\hat{z}$ is reliable, see also Section 3.1.

3.2.2. Task-flexible feedforward for point-of-interest control

In this section, the feedforward signal is parameterized in terms of the task r_j to achieve task-flexible feedforward. In particular, the feedforward signal is parameterized as a function of the task r_j as

$$f_j = F(\theta_j) r_j \tag{10}$$

where $F : \mathbb{R}^{n_\theta} \to \mathbb{R}^{N \times N}$ is defined in Definition 3.1. Ideally, $F(\theta_j)$ is designed such that it minimizes the actual point-of-interest error of (2) for all r, i.e., $e^z_j = 0$, as shown by

$$F(\theta_j) = \left(P^z\right)^{-1} + \left(\left(P^z\right)^{-1} P^y - 1\right) C, \tag{11}$$

which is derived from the substitution of (10) into (2). Indeed, the feedback controller C and the dynamics P^y, P^z influence the ideal feedforward, as such, the feedforward is a function of the feedback controller. In case a traditional non-inferential control setting is assumed, i.e., $P^y = P^z$, then $F(\theta_j) = \left(P^z\right)^{-1}$ leads to zero reference-induced error.

As is evident from the forthcoming simulation and experimental sections, the considered wirebonder, as well as general mechatronic systems, are modeled using rational models and feedback controllers that contain both poles and zeros. As a result, the transfer function of $F(\theta_j)$, $F(z, \theta_j)$, consists of rational basis functions, see Definition 3.1. Hence, a rational $F(z, \theta_j)$ can accurately describe (11) to obtain high tracking accuracy at the point of interest and flexibility in the motion task.

Definition 3.1 (*Rational Basis Functions*)**.** The rational feedforward parameterization is defined as

$$F(z, \theta_j) = A(z, \theta_j) B^{-1}(z, \theta_j), \tag{12}$$

with

$$A(z, \theta_j) = \xi^A_0(z) + \sum_{i=1}^{n_\theta} \xi^A_i(z) \theta_j[i], \tag{13a}$$

$$B(z, \theta_j) = \xi^B_0(z) + \sum_{i=1}^{n_\theta} \xi^B_i(z) \theta_j[i], \tag{13b}$$

where $\xi^A_i(z), \xi^B_i(z), i = 0, 1, \dots, n_\theta$ are user-defined polynomial transfer functions in complex indeterminate z, and ξ^B_0 constraints the denominator polynomial to be monic to guarantee the rational structure of $F(\theta_j)$ is well defined for all $\theta_j \in \mathbb{R}^{n_\theta}$. There exists Ψ^A_x and Ψ^B_x, with $\Psi^*_x = [\xi^*_1 x, \xi^*_2 x, \dots \xi^*_{n_\theta} x]$, where ξ^*_i is the convolution matrix of $\xi^*_i(z)$, such that $A(\theta_j)x = \xi^A_0 x + \Psi^A_x \theta_j$ and $B(\theta_j)x = \xi^B_0 x + \Psi^B_x \theta_j$, where $A(\theta_j)$ and $B(\theta_j)$ are the convolution matrices of $A(z, \theta_j)$ and $B(z, \theta_j)$, respectively.

Remark 3. Polynomial basis functions are recovered in case $B(z, \theta_j) = 1$, i.e., $f_j = F(\theta_j) r_j = \Psi(r_j)\theta_j$, which relates to FIR parameterizations depending on the choice of ξ^A_i, see [13,24], and [11]. Furthermore, the choice of n_θ is an order selection problem, similar to typical system identification approaches.

Now, substitution of the feedforward parameterization (10) into the predicted error propagation (9) yields

$$\tilde{e}^{\hat{z}}_{j+1} := e^{\hat{z}}_j + \hat{S}\hat{P}^z f_j - \hat{S}\hat{P}^z A(\theta_{j+1}) B^{-1}(\theta_{j+1}) r_{j+1}, \tag{14}$$

which can be iteratively minimized to learn θ_{j+1}. In order to do so, the next section presents the optimization problem and its solution for rational basis functions ILC in point-of-interest control, utilizing this predicted error propagation.

3.2.3. ILC solution for point-of-interest control

The objective in RBF ILC is to minimize the predicted error propagation through the following cost function.

Definition 3.2 (*Cost Function for RBF ILC for Point-of-interest Control*)**.** The cost function for RBF ILC for point-of-interest control using sensor fusion given the feedforward parameterization of Definition 3.1 is defined as

$$\begin{aligned}J_j(\theta_{j+1}) := \|\tilde{e}^{\hat{z}}_{j+1}(\theta_{j+1})\|^2_{W_e} + \|f_{j+1}(\theta_{j+1})\|^2_{W_f} \\ + \|f_{j+1}(\theta_j) - f_j\|^2_{W_{\Delta f}},\end{aligned} \tag{15}$$

where $W_e \succ 0$ and $W_f, W_{\Delta f} \succeq 0$ are weighting matrices that specify weighting for accuracy, robustness with respect to model uncertainty, and sensitivity to trial varying disturbances, respectively. Moreover, $\tilde{e}^z_{j+1}$ is defined in (9) and depends on feedforward f_j, sensor fusion estimate $\hat{z}_j$, and on the approximate models $\hat{P}^y, \hat{P}^z$.

The optimal feedforward parameters that minimize this cost function, i.e., minimize the estimated error of the next trial, are given by

$$\theta_{j+1}^{\text{opt}} := \underset{\theta_{j+1}}{\operatorname{argmin}}\, \mathcal{J}_j(\theta_{j+1}). \tag{16}$$

The cost function of (15) is in general non-convex in θ_{j+1}, hence finding the solution of (16) is non-trivial. To derive a solution, an iterative scheme is employed, as first derived in [15] for the case $P^y = P^z$, where the gradient

$$\frac{\mathrm{d}\mathcal{J}_j(\theta_{j+1})}{\mathrm{d}\theta_{j+1}} = 0 \tag{17}$$

is solved using an iterative scheme. The nonlinear terms in (17) are fixed in each numerical iteration $\langle k \rangle$ using the results of the previous iteration $\langle k-1 \rangle$. The iterative solution for $\theta_{j+1}^{\langle k \rangle}$ is given by

$$\theta_{j+1}^{\langle k \rangle} = L^{\langle k-1 \rangle} e_j^{\hat{z}} + Q^{\langle k-1 \rangle} f_j - R^{\langle k-1 \rangle} r_j, \tag{18}$$

where $L^{\langle k \rangle}$, $Q^{\langle k \rangle}$, and $R^{\langle k \rangle}$ are given in (A.1a) in Appendix A. Thus, a series of weighted least-squares problems is solved for each ILC iteration j. In Algorithm 1, the RBF ILC algorithm for point-of-interest control is presented that enables the computation of $\theta_{j+1}^{\text{opt}}$.

Algorithm 1 RBF ILC algorithm for point-of-interest control

Define: $\xi_i^A(z), \xi_i^B(z), i = 0, 1, \ldots, n_\theta$, G, and r_j.
Set: $j = 0$, θ_0, and ω_{co}.
while θ_j not converged **do**
  Determine $f_j = A(\theta_j)B^{-1}(\theta_j)r_j$.
  Perform an experiment with r_j and f_j and measure $\ddot{z}_j$ and y_j, as in Fig. 2.
  Perform sensor fusion to determine $\hat{z}_j$ using (4).
  Determine estimated tracking error $e_j^{\hat{z}}$ using (5).
  Set $k = 1$ and $\theta_{j+1}^{\langle 0 \rangle} = \theta_j$.
  while $k \leq k_{\max}$ **do**
    Determine $L^{\langle k-1 \rangle}$, $Q^{\langle k-1 \rangle}$, and $R^{\langle k-1 \rangle}$, see (A.1a) in Appendix A.
    Compute $\theta_{j+1}^{\langle k \rangle}$ using (18).
    $k \to k+1$.
  end while
  Set $\theta_{j+1} = \theta_{j+1}^{\langle k_{\max} \rangle}$.
  $j \to j+1$.
end while
Output: $\theta = \theta_j$

The following remarks should be made regarding the algorithm. First, in case $F(\theta_j)$ is unstable and possibly leads to unbounded f_j, stable inversion [25] approaches can be employed, which see the unstable filter as a non-causal operator. Second, the approach is similar to [15,26] for the non-inferential case, i.e., $P^y = P^z$. The differences due to the inferential control setting and use of sensor fusion are clearly visible in (9). Third, if the algorithm to find a minimum is convergent, the solution is a local optimum, as explained in [15]. Fourth, iteratively solving the non-convex optimization problem using a gradient-based weighting is closely related to instrumental-variable-based system identification, see, e.g., [16]. Fifth, regarding inferential control using ILC, there exists a potential conflict between the feedback and feedforward controller that could lead to unbounded growth of signals in case of an integral action in the feedback controller and depending on the chosen basis functions. This conflict can be easily eliminated by using a serial feedforward configuration instead of the parallel structure of Fig. 2, see [5]. However, for systems that satisfy Assumption 2 or when using sensor fusion that relies on the encoder measurement in the low-frequency range, the potential conflict in the parallel setting is not detrimental. Sixth, the convergence of Algorithm 1 depends on the model quality, as is standard in ILC algorithms, where the model has to be sufficiently good for convergence. Since basis functions are used, the convergence properties are typically automatically met, see [4], where the analysis can be directly extended to deal with the point-of-interest case.

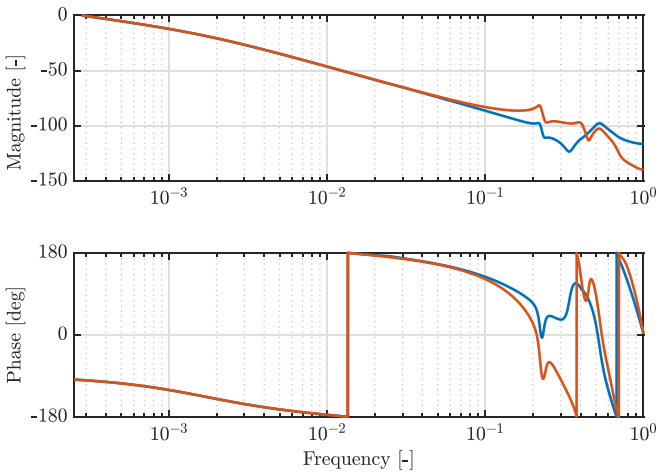

Fig. 4. Normalized Bode diagrams of the encoder dynamics P^y (—) and point-of-interest dynamics P^z (—) of the Simscape Multibody simulation model. Clearly, Assumption 2 holds and note that the low-frequency vibration caused by the reaction forces is slightly visible in the phase at a frequency of $2.5 \cdot 10^{-2}$.

4. Simulation study

To investigate the performance of the estimation using sensor fusion and optimization using RBF ILC, a simulation study is performed. The key idea is to use a representative simulation model, where the true performance can be directly measured. As such, it allows to investigate and compare the performance of both sensor fusion and the learning algorithm. This constitutes Contribution III of the paper.

4.1. Simulation setup

The simulation setup is a realistic Simscape Multibody model of a wirebonder by ASMPT, see Fig. 1, which includes a reduced-order FEM model for the bond head. Here, the lateral deflection of the bond head, illustrated in Fig. 3, limits the accuracy of the bonding process. Consequently, the analysis focuses solely on this specific motion axis. The position of the bond head in this motion direction represents the unmeasured performance variable, and the measured variable and the input are located elsewhere. Moreover, a low-frequency vibration caused by reaction forces is expected to be the highest contributor to the tracking error, hence the low-frequency performance of estimation using sensor fusion and compensation using rational feedforward will be the focus of this analysis. Due to the use of an actual commercial wirebonder, no machine details are presented and all results are normalized.

The linearized dynamics of the encoder measurement and the actual point of interest are shown in Fig. 4 and indicate that Assumption 2 is satisfied, i.e., the rigid-body dynamics at low frequencies have an identical response. The first resonance mode shows a large discrepancy between P^y and P^z, which is highly representative for the true system, see Fig. 8. The reference shown in Fig. 5 consists of four concatenated point-to-point motions with different motion distances and maximum accelerations. This concatenated motion task has a broad frequency content which is encountered in bonding tasks to ensure the learned feedforward really is task flexible. Both the encoder and acceleration measurements have added white noise of the same variance as encountered in the real setup. A stabilizing and high-performance feedback

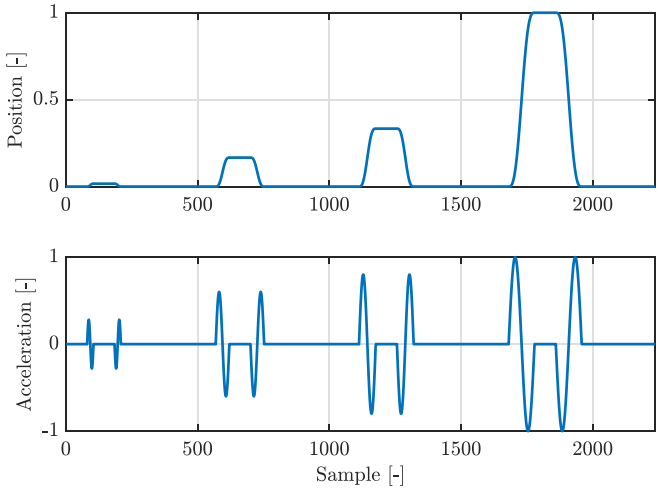

Fig. 5. Reference position and acceleration consisting of four concatenated point-to-point motions with different motion distances and maximum accelerations used in the simulation.

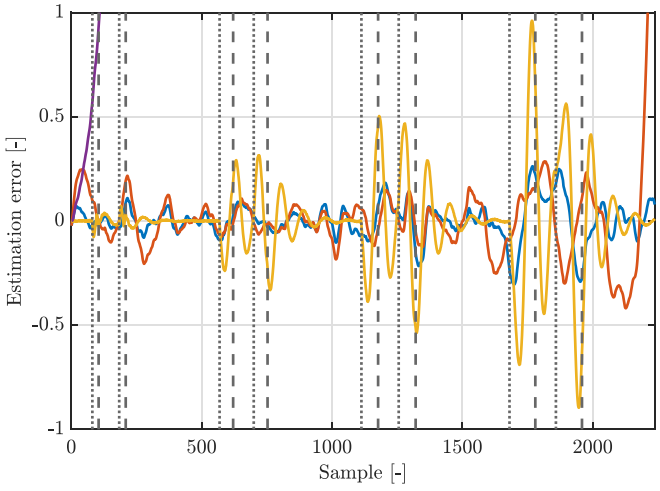

Fig. 6. Normalized estimation performance when neglecting point-of-interest dynamics, i.e., $y_j - z_j$ (—), using a double integrated acceleration measurement, i.e., $\tilde{z}_j - z_j$ (—), and the estimation error of the complementary filters, i.e., $\hat{z}_j - z_j$, with cross-over frequencies $7.5{\cdot}10^{-3}$ (—) and $3.7{\cdot}10^{-3}$ (—). Vertical lines indicate the start of the motion (⋯) and the end (– –). The sensor fusion approaches effectively remove drift from $\tilde{z}_j$, but the complementary filter with cross-over frequency $7.5 \cdot 10^{-3}$ achieves superior estimation performance.

controller is used to close the loop on the encoder measurement. Next, the estimation performance is analyzed.

4.2. Estimation performance

To analyze the estimation performance of sensor fusion with respect to the actual point-of-interest and highlight the sensitivity of the cross-over frequency, two complementary filters are designed. The filters consist of a matching pair of third-order low-pass and high-pass Butterworth filters with cross-over frequency $7.5 \cdot 10^{-3}$ and $3.7 \cdot 10^{-3}$. These frequencies are chosen with the following principle in mind. The low-frequency base frame vibration is the upper bound for the cross-over frequency of the complementary filter, as the dynamics P^y and P^z start to deviate at that frequency. The lower bound is the frequency where the drift from double integration acceleration data with noise is effectively removed from the estimated signal. Moreover, high-frequency measurement noise is removed from the acceleration signal, and zero-phase filtering is employed for the complementary filters.

The estimation performance is evaluated with respect to the actual point of interest z_{10}, which is only available in simulation, in trial $j = 10$ for the case of near-perfect tracking in the encoder variable using standard norm-optimal ILC [10]. Initially, relying solely on the encoder measurement y_{10} as an estimate for the point of interest, i.e., neglecting the dynamics of the point of interest, reveals a significant discrepancy. This is illustrated in Fig. 6 by the substantial estimation error $y_j - z_j$, which highlights the need for an accurate estimate of the point of interest. Subsequently, employing the double integrated acceleration measurement $\tilde{z}_{10}$, see (3), as an estimation of the point of interest results in drift in the estimation error $\tilde{z}_{10} - z_{10}$, which emphasizes the need for sensor fusion techniques. Finally, the estimation error $\hat{z}_{10} - z_{10}$ of the complementary filter with frequency $3.7 \cdot 10^{-3}$ has better performance than the naive encoder measurement $y_{10} - z_{10}$, but still shows some drift, especially before and after the motions. The complementary filter with frequency $7.5 \cdot 10^{-3}$ has superior performance, possibly due to its proximity to the lower boundary for drift removal. The differences in performance between the two complementary filters clearly highlights the sensitivity to the cross-over frequency and shows that sensor fusion can be effective for the removal of drift in $\tilde{z}$. Since the complementary filter with the higher cross-over frequency of $7.5 \cdot 10^{-3}$ shows overall superior performance, this filter is selected for the remainder of this work.

4.3. Tracking performance

The tracking performance, in terms of the actual tracking error of the point of interest, of rational basis functions ILC is analyzed by comparison of using three different RBF ILC minimization variables, namely, the encoder error e_j^y, the sensor fusion estimation of the point of interest error $e_j^{\hat{z}}$ with cross-over frequency $7.5 \cdot 10^{-3}$, and the true point of interest error e_j^z, which is thus not estimated and only available in simulation.

The procedure for RBF ILC to minimize e_j^y is derived from Alg 1 by setting $P^z = P^y$ and replacing $e^{\hat{z}}$ in (9) with $e^y = r_j - y_j$, and the procedure to minimize for e_j^z is derived by only replacing $e^{\hat{z}}$ in (9) with e_j^z. For each method, the weighting matrices of (15) are selected as $W_e = I$ and $W_f = W_{\Delta f} = 0$ since the ILC algorithm in Alg 1 converges without requiring $W_f > 0$ since there are negligible model mismatches and trial-varying disturbances in the simulation. The algorithms use $k_{\max} = 25$ offline iterations. A fixed rigid-body feedforward is already implemented, and the rational feedforward parameterization is added in parallel but as a function of $\ddot{r}_j$, i.e. ,

$$f_j = K_v \dot{r}_j + K_a \ddot{r}_j + F(\theta_j)\ddot{r}_j \tag{19}$$

where K_v, K_a are the viscous friction and acceleration parameter, respectively, and $\dot{r}_j$ and $\ddot{r}_j$ are the continuous-time derivatives of the generated reference $r_j(t)$, e.g., obtained via $\ddot{r}_j[k] = \left(\frac{\mathrm{d}^2}{\mathrm{d}t^2} r(t)\right)[kT_s]$. This approach is essentially the same as described in Definition 3.1, but with a fixed rigid-body part already implemented, and the rational structure focuses only on the higher-order flexible dynamics by using $\ddot{r}_j$ instead of r_j. Delays in the feedforward signal are avoided by using continuous-time derivatives. The feedforward parameterization $F(\theta_j)$ of Definition 3.1 is constructed with $\xi_i^A(z) = \{0,\ 1,\ (1-z^{-1}),\ (1-z^{-1})^2,\ 0,\ 0\}_0^{n_\theta}$ and $\xi_i^B(z) = \{1,\ 0,\ 0,\ 0,\ (1-z^{-1}),\ (1-z^{-1})^2\}_i^{n_\theta}$, with $n_\theta = 5$. Moreover, time-advancing of the feedforward signal is performed to compensate for delays in the simulated system.

A comparison of the normalized errors in the encoder and the point of interest for each RBF ILC minimization variable, e_j^y, $e_j^{\hat{z}}$, and e_j^z, is presented in Fig. 7. Initially, when optimizing for e_j^y, the encoder tracking error is significantly reduced, but this leads to a substantial increase in the point-of-interest tracking error, which is primarily due

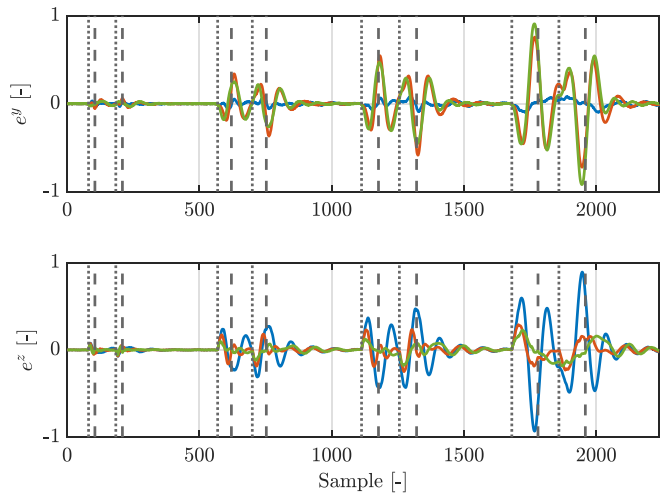

Fig. 7. Normalized error in the encoder e^y (top) and error in the actual point of interest e^z (bottom) for RBF ILC that minimizes for e_j^y (—), $e_j^{\hat{z}}$ with cross-over frequency $7.5 \cdot 10^{-3}$ (—), and the true point of interest error e_j^z (—). Vertical lines indicate motion start (⋯) and end (– –). Sensor fusion, albeit an imperfect estimate, enables high point-of-interest tracking accuracy on par with using the true point-of-interest error for optimization.

to the low-frequency vibrations caused by the reaction forces. On the contrary, optimizing for $e_j^{\hat{z}}$ through sensor fusion significantly improves the point-of-interest error by effectively compensating for these low-frequency vibrations. However, this approach does amplify the errors in the encoder, which is expected. Moreover, a comparison between minimizing for $e_j^{\hat{z}}$ and e_j^z reveals that, despite imperfect estimation, using sensor fusion for the estimation results in a point-of-interest tracking accuracy comparable to that achieved when the true point-of-interest error is used for optimization.

5. Experimental validation

In this section, the developed RBF ILC algorithm for point of interest control using sensor fusion is validated on a commercial wirebonder by ASMPT, which constitutes contribution IV. Similarly as in the simulation, the tracking performance of RBF ILC is analyzed by comparing optimizing for the encoder error e_j^y with optimizing for the sensor fusion estimation of the point-of-interest error $e_j^{\hat{z}}$. This constitutes Contribution IV of this paper.

5.1. Experimental setup

The experiments are performed on a commercial wirebonder by ASMPT, see Fig. 1. Similarly to the simulations, the lateral deflection of the bond head is considered, as shown in Fig. 3. To enable estimation of the unmeasured performance variable, an accelerometer is added at the tip of the bond head and connected to an analog-to-digital converter via flexible wires, satisfying Assumption 1 about approximate unaltered dynamics. A typical and commonly-used-in-industry calibration procedure is performed to digitally align the axis of the accelerometer with the axis of motion of the bond head. Frequency response function (FRF) measurements are performed for both the encoder and the point of interest, and are shown in Fig. 8. Deviations around the resonance frequencies confirm that the bond head indeed substantially deforms, and these frequencies are excited by the fast reference signals that are being used. Three aspects are considered important. First, qualitatively, the system behavior is in-line with the simulation model, see Fig. 4, hence the simulation study is highly representative. Second, the sensor fusion algorithm does not depend on any model, only the fact that there

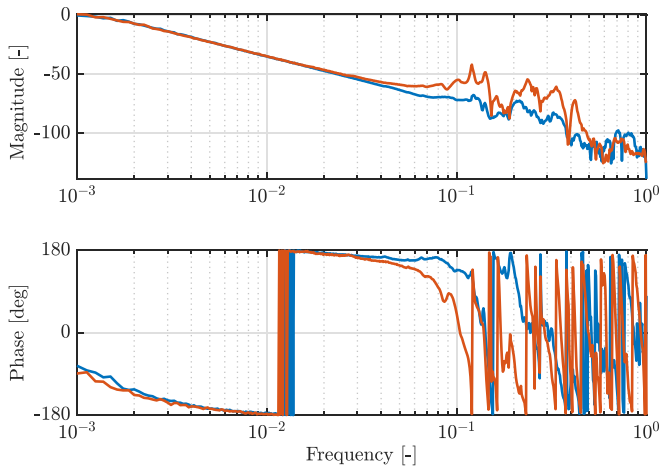

Fig. 8. Normalized Bode diagrams of the FRF measurements of the encoder (—) and the point of interest (—).

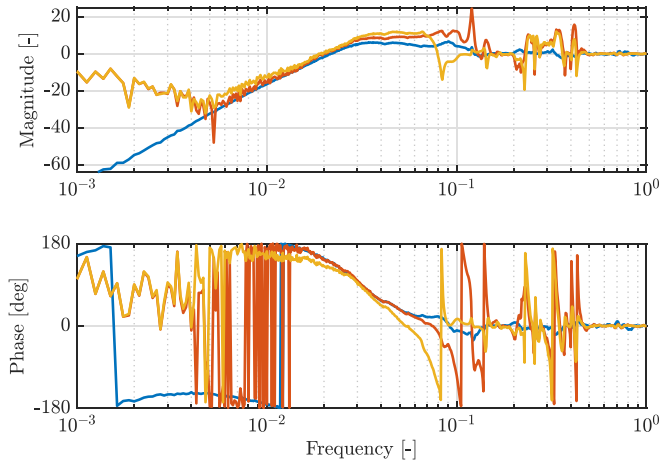

Fig. 9. Normalized Bode diagrams of the encoder sensitivity $r \to e^y$ (—) and the point-of-interest sensitivity $r \to e^z$ (—), both with the feedback controller designed for the encoder, and the point-of-interest sensitivity $r \to e^z$ with the redesigned feedback controller for the point of interest (—).

is a difference between P^y and P^z in the high frequency region. Third, ILC does require a reasonably accurate model to establish convergence. To this end, low-order parametric models $\hat{P}^y, \hat{P}^z$ are fitted to these FRFs and used for the ILC algorithm. Moreover, albeit not visible in the FRF measurements, the low-frequency vibration caused by reaction forces is again expected to be the leading contributor in the tracking error and in this machine multiple flexible modes are expected. The reference shown in Fig. 5 is again used during all experiments, and a high-bandwidth feedback controller is designed based on the FRF of the encoder. The FRF of the sensitivity $S : r \to e^y$ and the FRF of the point-of-interest sensitivity $S^z := (1 - SP^zC) : r \to e^z$, see (2), are shown in Fig. 9. Clearly, amplification of frequencies in the point of interest is present due to the high-bandwidth feedback controller, which will be dealt with later on by redesigning the feedback controller. Note that the accuracy of the point-of-interest sensitivity at low frequencies could be improved by employing frequency-domain sensor fusion. For confidentiality reasons, no further machine details are presented and all results are normalized.

5.2. Design aspects

The sensor fusion and ILC algorithm are set up as follows. The complementary filter with the cross-over frequency of $7.5 \cdot 10^{-3}$ is

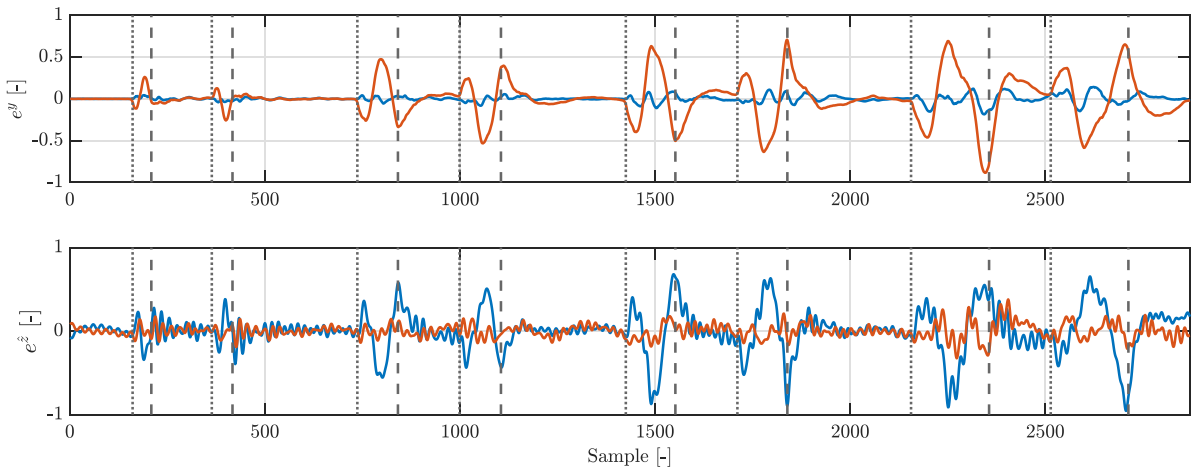

Fig. 10. Normalized error in the encoder e^y (top) and error in the estimated point of interest $e^{\hat{z}}$ (bottom) for RBF ILC that minimizes for e_j^y (—) and $e_j^{\hat{z}}$ with cross-over frequency $7.5 \cdot 10^{-3}$ with the feedback controller designed for the encoder (—). Vertical lines indicate the start of the motion (⋯) and the end (– –). The tracking error in the point of interest is significantly improved via the developed framework compared to minimizing the encoder error. The high-frequency oscillations appear to correspond to the amplifications in $r \to e^z$ from Fig. 9.

also chosen for the experiments because it effectively removes drift and is expected to yield the best estimation performance. Again, the filter consists of a matching pair of third-order low-pass and high-pass Butterworth filters. Moreover, high-frequency measurement noise is removed from the acceleration signal, and zero-phase filtering is employed for the complementary filter.

Regarding the ILC setup, the weighting matrices of (15) are selected as $W_e = I$ and $W_f = 10^{-12} \cdot I$, which avoids aggressive feedforward signals, and $W_{\Delta f} = 0$ since trial-varying disturbances, such as noise, are sufficiently low. The algorithms use $k_{\max} = 45$ offline iterations to ensure convergence of the feedforward parameters. Again, a fixed rigid-body feedforward is already implemented, and the rational feedforward parameterization is added in parallel as described in (19). However, to facilitate the compensation of multiple flexible modes, the feedforward parameterization $F(\theta_j)$ of Definition 3.1 is now extended to $\xi_i^A(z) = \{0,\ 1,\ (1-z^{-1}),\ (1-z^{-1})^2,\ (1-z^{-1})^3,\ (1-z^{-1})^4,\ 0,\ 0,\ 0,\ 0\}_0^{n_\theta}$ and $\xi_i^B(z) = \{1,\ 0,\ 0,\ 0,\ 0,\ 0,\ (1-z^{-1}),\ (1-z^{-1})^2,\ (1-z^{-1})^3,\ (1-z^{-1})^4\}_0^{n_\theta}$, with $n_\theta = 9$. Moreover, time-advancing of the feedforward signal is performed to compensate for delays in the system. Furthermore, input saturation compensation is applied on the feedforward, see [27] for derivation and explanation.

5.3. Results

A comparison of the normalized errors in the encoder and the point of interest for the RBF ILC minimization variable, e_j^y and $e_j^{\hat{z}}$, presented in Fig. 10, clearly reveals that optimizing for the estimated point of interest error, $e_j^{\hat{z}}$, results in a significantly lower estimated point-of-interest error compared to minimizing the encoder error e_j^y. This optimization strategy also achieves a 2.7 times lower 2-norm for the estimated point of interest error. Moreover, similar to the conclusion of Section 4, optimizing for the estimated point of interest error $e_j^{\hat{z}}$ yields a substantial higher error in the encoder error e^y. It should be noted that the point-of-interest error is still an estimation and validation through absolute position measurements is a logical next step. Moreover, high-frequency oscillations are present in the estimated point of interest error that correspond to the amplifications in $r \to e^z$ from Fig. 9 at frequencies of 0.1 and 0.12, suggesting that these could be attenuated with a feedback controller designed that takes the point of interest dynamics into account, as presented next.

5.4. Attenuating oscillations

In an attempt to attenuate the high-frequency oscillation present in the error and to isolate the origin of these, the feedback controller is redesigned taking into account the dynamics of the point of interest. The sensitivity of the point of interest $r \to e^z$ is shown in Fig. 9 and shows high attenuation of frequencies of 0.1 and 0.12. Now, to isolate the effect of the feedback controller on these oscillations, polynomial basis functions ILC is performed, i.e., $F(\theta_j) = 0$ and only K_v, K_a in (19) are optimized by ILC, since the rational feedforward controller could also attenuate these frequencies. Furthermore, the possible effects of ILC on these oscillations are further reduced by optimizing for the encoder error e_j^y, since these oscillations are only present in the sensor fusion estimate of the tracking error $e_j^{\hat{z}}$. The estimated point-of-interest tracking error for the new feedback controller redesigned for the point of interest is Fig. 11. The oscillations are only slightly attenuated, indicating that the oscillations are not caused by the feedback controller of the considered motion axis. A possible explanation for these oscillations might be that vibrations in other motion directions are present in the considered motion axis through incorrect rotation calibration of the accelerometer.

6. Conclusions

The developed framework enables accurate estimation and control of the unmeasured performance variables through sensor fusion and task-flexible feedforward control. In particular, the sensor fusion of the measured variable and a temporary acceleration measurement of the unmeasured performance variable via a complementary filter provides a reliable estimate of the point of interest tracking error. Subsequently, the developed approach for task-flexible feedforward for the point of interest minimizes the estimated tracking error via rational basis functions ILC for point-of-interest control. The simulation results show that, despite the imperfect estimation, the application of sensor fusion for the estimation results in a point-of-interest tracking accuracy that is comparable to that achieved when the true point-of-interest error is used for optimization. Moreover, experimental validation on a wirebonder machine shows that optimizing for the estimated point-of-interest error results in a significantly lower estimated point of interest error compared to minimizing the encoder error. As a consequence, the end-user of the machine now has full control over the servo performance of the point of interest, and can specify the reference in such a way that optimizes the overall system performance.

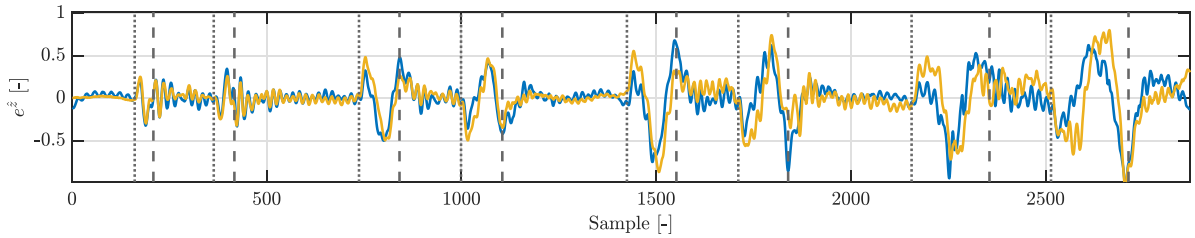

Fig. 11. Normalized error in the estimated point of interest $e^{\hat{z}}$ for polynomial basis functions ILC that minimizes for e_j^y with the original feedback controller designed for the encoder (—) and with the new feedback controller designed for the point of interest (—). Vertical lines indicate the start of the motion (⋯) and the end (- -). The high-frequency oscillations are only slightly attenuated by the new feedback controller, indicating that the oscillations are not caused by the feedback controller.

Directions for future research include isolating the origin of the oscillations present in the estimation of the point of interest and validating the sensor fusion estimate with an absolute position measurement. Furthermore, a broader use of the presented sensor fusion approach, e.g., a causal approach for enhanced feedback design for disturbance suppression are possibly highly relevant for precision mechatronic and robotic systems.

From a broader perspective, our results indicate the application and industrial relevance of point of interest performance in high performance systems. Explicitly addressing such variables may be of major importance in other control algorithms, including data-driven optimization algorithms, such as repetitive control or iterative feedback tuning.

CRediT authorship contribution statement

Maurice Poot: Writing – review & editing, Writing – original draft, Visualization, Validation, Software, Methodology, Investigation, Formal analysis, Data curation, Conceptualization. **Jorrit Sprik:** Visualization, Validation, Software, Methodology, Investigation, Data curation. **Matthijs Teurlings:** Software, Methodology, Investigation, Formal analysis, Conceptualization. **Wout Laarakkers:** Visualization, Validation, Software, Resources, Methodology, Data curation. **Dragan Kostić:** Writing – review & editing, Writing – original draft, Supervision, Project administration, Methodology, Investigation, Validation, Resources, Formal analysis, Data curation, Conceptualization . **Jim Portegies:** Writing – review & editing, Visualization, Supervision, Methodology, Formal analysis. **Tom Oomen:** Writing – review & editing, Supervision, Resources, Project administration, Funding acquisition, Conceptualization.

Declaration of competing interest

The authors declare the following financial interests/personal relationships which may be considered as potential competing interests: Maurice Poot reports financial support was provided by ASM Pacific Technology Pte Ltd. If there are other authors, they declare that they have no known competing financial interests or personal relationships that could have appeared to influence the work reported in this paper.

Acknowledgments

The authors gratefully acknowledge the contribution of Jilles van Hulst, (Kelvin) Kai Wa Yan, Mojtaba Haghi, and Jasper Gerritsen.

Appendix A. RBF ILC for point-of-interest control

The solution of the RBF ILC algorithm for point-of-interest control using the error propagation of (9) is derived by fixing the nonlinear terms in the gradient in each numerical iteration $\langle k \rangle$ using the results of the previous iteration $\langle k-1 \rangle$. By equation the gradient to zero, the matrices $L^{\langle k-1 \rangle}, Q^{\langle k-1 \rangle}$, and $R^{\langle k-1 \rangle}$, are computed as

$$L^{\langle k-1 \rangle} = \left(\zeta^{\langle k-1 \rangle} \Gamma\right)^{-1} \zeta^{\langle k-1 \rangle} \left(\hat{S}\hat{P}^z\right)^\top W_e \xi_0^B, \tag{A.1a}$$

$$Q^{\langle k-1 \rangle} = \left(\zeta^{\langle k-1 \rangle} \Gamma\right)^{-1} \zeta^{\langle k-1 \rangle} \left(\left(\hat{S}\hat{P}^z\right)^\top W_e \hat{S}\hat{P}^z + W_{\Delta f}\right) \xi_0^B, \tag{A.1b}$$

$$R^{\langle k-1 \rangle} = \left(\zeta^{\langle k-1 \rangle} \Gamma\right)^{-1} \zeta^{\langle k-1 \rangle} \left(\left(\hat{S}\hat{P}^z\right)^\top W_e \hat{S}\hat{P}^z + W_f + W_{\Delta f}\right) \xi_0^A, \tag{A.1c}$$

where

$$\begin{aligned} \Gamma := &\left(\left(\hat{S}\hat{P}^z\right)^\top W_e \hat{S}\hat{P}^z + W_f + W_{\Delta f}\right) \Psi_{r_j}^A \\ &- \left(\hat{S}\hat{P}^z\right)^\top W_e \Psi_{e_j}^B - \left(\left(\hat{S}\hat{P}^z\right)^\top W_e \hat{S}\hat{P}^z + W_{\Delta f}\right) \Psi_{f_j}^B, \end{aligned} \tag{A.2}$$

and

$$\zeta^{\langle k-1 \rangle} = \left(\frac{\mathrm{d} f_{j+1}^{\langle k-1 \rangle}}{\mathrm{d}\theta_{j+1}^{\langle k-1 \rangle}}\right)^\top B^{-1}\left(\theta_{j+1}^{\langle k-1 \rangle}\right), \tag{A.3}$$

with

$$\frac{\mathrm{d} f_{j+1}^{\langle k-1 \rangle}}{\mathrm{d}\theta_{j+1}^{\langle k-1 \rangle}} = B^{-1}\left(\theta_{j+1}^{\langle k-1 \rangle}\right) \Psi_{r_j}^A - A\left(\theta_{j+1}^{\langle k-1 \rangle}\right) B^{-2}\left(\theta_{j+1}^{\langle k-1 \rangle}\right) \Psi_{r_j}^B. \tag{A.4}$$

The weighting matrices $W_e \succ 0$ and $W_f, W_{\Delta f} \succeq 0$ should be chosen such that $\zeta^{\langle k \rangle} \Gamma$ is full rank, which is already often the case for most rational feedforward parameterizations even when $W_f = W_{\Delta f} = 0$.

Appendix B. Zero-phase filtering using Butterworth filters

Zero-phase filtering [23] effectively squares the magnitude of the original filter and removes the phase delay. The squared magnitudes of a low- and high-pass Butterworth filter of order n are

$$|G_{\mathrm{LP}}(j\omega)|^2 = \frac{1}{1 + \left(\frac{\omega}{\omega_{\mathrm{co}}}\right)^{2n}}, \tag{B.1a}$$

$$|G_{\mathrm{HP}}(j\omega)|^2 = \frac{1}{1 + \left(\frac{\omega_{\mathrm{co}}}{\omega}\right)^{2n}}, \tag{B.1b}$$

where $\omega_{\mathrm{co}} = 2\pi f_{\mathrm{co}}$ is the cut-off frequency [28]. Now, summing these magnitudes yields

$$\frac{2 + \left(\frac{\omega}{\omega_{\mathrm{co}}}\right)^{-2n} + \left(\frac{\omega}{\omega_{\mathrm{co}}}\right)^{2n}}{1 + \left(\frac{\omega}{\omega_{\mathrm{co}}}\right)^{-2n} + \left(\frac{\omega}{\omega_{\mathrm{co}}}\right)^{2n} + \left(\frac{\omega}{\omega_{\mathrm{co}}}\right)^{-2n}\left(\frac{\omega}{\omega_{\mathrm{co}}}\right)^{2n}} = 1. \tag{B.2}$$

Data availability

The data that has been used is confidential.

References

[1] Parrish JR, Brosilow CB. Inferential control applications. Automatica 1985;21(5):527–38.
[2] Wallén J, Norrlöf M, Gunnarsson S. A framework for analysis of observer-based ILC. Asian J Control 2011;13(1):3–14. http://dx.doi.org/10.1002/asjc.261.
[3] Oomen T, Grassens E, Hendriks F. Inferential motion control: Identification and robust control framework for positioning an unmeasurable point of interest. IEEE Trans Control Syst Technol 2015;23(4):1602–10. http://dx.doi.org/10.1109/TCST.2014.2371830.
[4] Boeren F, Bareja A, Kok T, Oomen T. Frequency-domain ILC approach for repeating and varying tasks: With application to semiconductor bonding equipment. IEEE/ASME Trans Mechatronics 2016;21(6):2716–27.
[5] Bolder J, Oomen T. Inferential iterative learning control: A 2D-system approach. Automatica 2016;71:247–53. http://dx.doi.org/10.1016/j.automatica.2016.04.029.
[6] van Zundert J, Oomen T. On optimal feedforward and ILC: The role of feedback for optimal performance and inferential control. IFAC-PapersOnLine 2017;50(1):6093–8. http://dx.doi.org/10.1016/j.ifacol.2017.08.1384.
[7] Oomen T, Van Herpen R, Quist S, Van De Wal M, Bosgra O, Steinbuch M. Connecting system identification and robust control for next-generation motion control of a wafer stage. IEEE Trans Control Syst Technol 2014;22(1):102–18. http://dx.doi.org/10.1109/TCST.2013.2245668.
[8] Blanken L, Boeren F, Bruijnen D, Oomen T. Batch-to-batch rational feedforward control: From iterative learning to identification approaches, with application to a wafer stage. IEEE/ASME Trans Mechatronics 2017;22(2):826–37. http://dx.doi.org/10.1109/TMECH.2016.2625309.
[9] Bristow D, Tharayil M, Alleyne A. A survey of iterative learning. EEE Control Syst Mag 2006;26(3):96–114.
[10] Gunnarsson S, Norrlöf M. On the design of ILC algorithms using optimization. Automatica 2001;37(12):2011–6. http://dx.doi.org/10.1016/S0005-1098(01)00154-6.
[11] van der Meulen SH, Tousain RL, Bosgra OH. Fixed structure feedforward controller design exploiting iterative trials: Application to a wafer stage and a desktop printer. J Dyn Syst Meas Control 2008;130(5):0510061–05100616. http://dx.doi.org/10.1115/1.2957626.
[12] Hoelzle D, Alleyne A, Wagoner Johnson A. Basis task approach to iterative learning control with applications to micro-robotic deposition. IEEE Trans Control Syst Technol 2011;19(5):1138–48. http://dx.doi.org/10.1109/TCST.2010.2063030.
[13] van de Wijdeven J, Bosgra O. Using basis functions in iterative learning control: analysis and design theory. Internat J Control 2010;83(4):661–75.
[14] Bolder J, Oomen T. Rational basis functions in iterative learning control - with experimental verification on a motion system. IEEE Trans Control Syst Technol 2015;23(2):722–9. http://dx.doi.org/10.1109/TCST.2014.2327578.
[15] van Zundert J, Bolder J, Oomen T. Optimality and flexibility in iterative learning control for varying tasks. Automatica 2016;67:295–302. http://dx.doi.org/10.1016/j.automatica.2016.01.026.
[16] Söderström T, Stoica P. Instrumental variable methods for system identification. Circuits Systems Signal Process 2002;21(1):1–9. http://dx.doi.org/10.1007/BF01211647.
[17] Gunnarsson S, Norrlöf M, Rahic E, Özbek M. On the use of accelerometers in iterative learning control of a flexible robot arm. Internat J Control 2007;80(3):363–73. http://dx.doi.org/10.1080/00207170600996518.
[18] Bolder J, Oomen T, Steinbuch M. On inferential iterative learning control: With example to a printing system. Proc Am Control Conf 2014;1827–32. http://dx.doi.org/10.1109/ACC.2014.6858946.
[19] Trimpe S, D'Andrea R. Accelerometer-based tilt estimation of a rigid body with only rotational degrees of freedom. Proc IEEE Int Conf Robot Autom 2010;2630–6.
[20] Welch G, Bishop G. An introduction to the Kalman filter. Chapel Hill, North Carolina; 1995.
[21] Sasiadek JZ. Sensor fusion. Annu Rev Control 2002;26 II(2):203–28. http://dx.doi.org/10.1016/S1367-5788(02)00045-7.
[22] Higgins W. A comparison of complementary and Kalman filtering. IEEE Trans Aerosp Electron Syst 1975;AES-11(3):321–5.
[23] Gustafsson F. Determining the initial states in forward-backward filtering. IEEE Trans Signal Process 1996;44(4):988–92. http://dx.doi.org/10.1109/78.492552.
[24] Bolder J, Oomen T, Koekebakker S, Steinbuch M. Using iterative learning control with basis functions to compensate medium deformation in a wide-format inkjet printer. Mechatronics 2014;24(8):944–53.
[25] van Zundert J, Oomen T. On inversion-based approaches for feedforward and ILC. Mechatronics 2018;50(September 2017):282–91. http://dx.doi.org/10.1016/j.mechatronics.2017.09.010.
[26] Bolder J, van Zundert J, Koekebakker S, Oomen T. Enhancing flatbed printer accuracy and throughput: Optimal rational feedforward controller tuning via iterative learning control. IEEE Trans Ind Electron 2017;64(5):4207–16. http://dx.doi.org/10.1109/TIE.2016.2613498.
[27] Poot M, Hulst JV, Yan KW, Kostić D, Portegies J, Oomen T. Feedforward control in the presence of input nonlinearities: With application to a wirebonder. In: Proceedings of the IFAC 22st triennial world congress. Yokohama, Japan; 2023, p. 2045–50.
[28] Mahata S, Saha SK, Kar R, Mandal D. Optimal design of fractional order low pass butterworth filter with accurate magnitude response. Digit Signal Process 2018;72:96–114. http://dx.doi.org/10.1016/j.dsp.2017.10.001.

Maurice Poot received the M.Sc. degree from the Eindhoven University of Technology in the Department of Mechanical Engineering in 2019. He received his Ph.D. degree in 2024 at the Eindhoven University of Technology in the Department of Mechanical Engineering. His research interests include Gaussian processes, data-driven learning, learning, and control with application to mechatronic systems.

Jorrit Sprik received the M.Sc. degree from the Eindhoven University of Technology in 2023 in the Department of Mechanical Engineering. His research interests include identification, data-driven learning, and control with application to mechatronic systems.

Matthijs Teurlings received his M.Sc. degree from the Eindhoven University of Technology in the Department of Mechanical Engineering in 2023. His research interests include learning control, modal system identification, embedded motion control, and control with application to mechatronic systems.

Wout Laarakkers received the M.Sc. degree from the Eindhoven University of Technology in the Department of Systems and Control in 2017. Working for the Centre of Competence of ASMPT his research activities include industrialization of control algorithms for mechatronic systems, Setpoint generation and shaping, and automated feedback turning.

Dragan Kostić received the Ph.D. degree in control technology and robotics from Eindhoven University of Technology, Eindhoven, The Netherlands, in 2004. He works at ASMPT, Beuningen, The Netherlands, as a Research and Development Director for mechatronics. His professional positions range from research and teaching at knowledge institutions to professional engineering in commercial companies. Multidisciplinary system modeling and identification, data-based controls, and nonlinear control designs are his main areas of expertise. His current research interests include modeling, dynamical analysis, and control of high-tech mechatronic systems for semiconductor manufacturing.

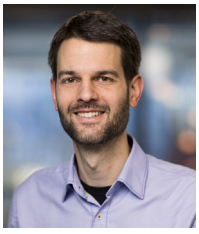

Jim Portegies obtained his M.Sc. degree in Industrial and Applied Mathematics and Applied Physics from the Eindhoven University of Technology in 2009. He spent the 2007-2008 academic year as an exchange student at the University of Bonn, Germany. He received his Ph.D. degree in Mathematics from the Courant Institute of Mathematical Sciences in New York. In the Fall of 2013, he spent a semester at NYU Shanghai, in Shanghai, China. After completing his Ph.D. in 2014, he spent two years a postdoc at the Max Planck Institute for Mathematics in the Sciences in Leipzig, Germany until he returned to the Eindhoven University of Technology as an assistant professor in Mathematics in 2016. He is also a member of The Young Academy of the KNAW.

Tom Oomen received M.Sc. degree (cum laude) and Ph.D. degree from the Eindhoven University of Technology, Eindhoven, The Netherlands. He is currently a full professor with the Department of Mechanical Engineering at the Eindhoven University of Technology. He is also a part-time full professor with the Delft University of Technology. He held visiting positions at KTH, Stockholm, Sweden, and at The University of Newcastle, Australia. His research interests are in the field of data-driven modeling, learning, and control, with applications in precision mechatronics. He is a recipient of the 7th Grand Nagamori Award, the Corus Young Talent Graduation Award, the IFAC 2019 TC 4.2 Mechatronics Young Research Award, the 2015 IEEE Transactions on Control Systems Technology Outstanding Paper Award, the 2017 IFAC Mechatronics Best Paper Award, the 2019 IEEJ Journal of Industry Applications Best Paper Award, and recipient of a Veni and Vidi personal grant. He is a Senior Member of Institute of Electrical and Electronics Engineers, he has been a Senior Editor of IEEE Control Systems Letters (L-CSS) and Co-Editor-in-Chief of IFAC Mechatronics, and he has served on the editorial board of IEEE Transactions on Control Systems Technology. He has also been vice-chair for IFAC TC 4.2 and a member of the Eindhoven Young Academy of Engineering.